ISSN 2007-9737

Classification of pH Status in Stevia Plants Using Supervised Neural Networks and Computer Vision

Jesús Emmanuel Brizuela-Ramírez[1], Noel García-Díaz[1,*], Juan García-Virgen[1], Shanti Maryse Gutiérrez-Magaña[1], Dewar Rico-Bautista[2]

[1] Tecnológico Nacional de México, Mexico

[2] Universidad Francisco de Paula Santander Ocaña, Mexico

{g2346011, ngarcia,jgarcia, g2346013}@colima.tecnm.mx, dwricob@ufpso.edu.com

Abstract. Artificial Intelligence and Computer Vision have revolutionized Precision Agriculture, enabling automated crop monitoring. This study proposes a model based on Neural Networks to classify soil pH in Stevia rebaudiana Bertoni crops, optimizing agricultural management and crop sustainability. To achieve this, Stevia images were processed using data augmentation techniques, extracting color features in RGB and hexadecimal formats. A supervised Artificial Neural Network was then trained to classify soil pH into acidic, optimal, and alkaline categories. The proposed model, StePHVIA, achieved 99% accuracy, outperforming pretrained architectures such as MobileNetV2 (97.38%) and ResNet-50 (76.38%). The evaluation was conducted using metrics such as Matthews Correlation Coefficient, accuracy, recall, and F1-score. These results confirm the effectiveness of Computer Vision and Deep Learning in Precision Agriculture, providing a real time and low cost alternative for soil monitoring. StePHVIA facilitates the early detection of soil imbalances, optimizing fertilizer application and improving Stevia crop productivity.

Keywords. Artificial Intelligence, computer vision, neural networks, precision agriculture, stevia.

1 Introduction

Artificial Intelligence (AI) has become increasingly important in agriculture by providing innovative tools to optimize production through data collection and analysis. Recent research has demonstrated that AI enhances precision in crop management and decision making efficiency by using machine learning (ML) algorithms and predictive analytics to assess plant health and predict resource demand [1, 2].

According to specialized literature [3], AI is defined as the capability of computational systems to perform tasks that traditionally require human intelligence, such as pattern recognition, decision making, and autonomous learning from data. Within this framework, Deep Learning (DL) algorithms enable machines to "learn" automatically from large volumes of data without the need for explicit programming for each task [4]. Similarly, predictive analytics employs historical data and mathematical models to anticipate future outcomes, which is particularly useful in agriculture for forecasting crop nutrient requirements and optimizing farm management [5].

Among the most widely used techniques in IA are Artificial Neural Network (ANN) [6], which have proven highly effective in various agricultural applications, such as detecting crop issues [7], classifying healthy and diseased plants [8], predicting crop yield [9], and optimizing the use of essential resources such as water [10] and fertilizers [11]. These characteristics make ANNs an essential tool in Precision Agriculture (PA), where improving efficiency and productivity is crucial to addressing the sector's current challenges.

A particularly relevant application of AI in agriculture is Computer Vision (CV), a technology that enables the precise identification of plant

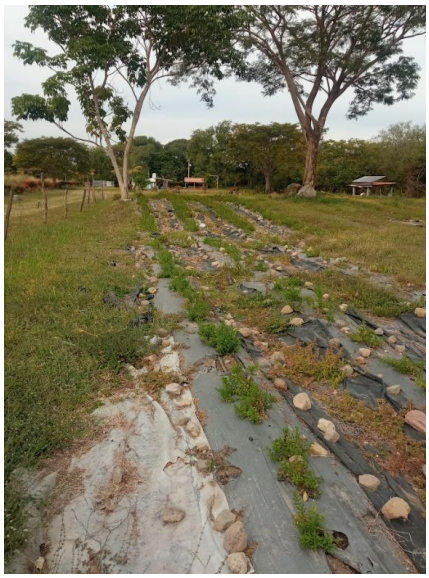

Fig. 1. Rancho Tajeli

issues through automated image analysis. Recent studies have demonstrated the effectiveness of CV in the early detection of crop alterations, facilitating the implementation of preventive and corrective strategies to minimize production losses [12,13,14]. According to [15], CV can assess visual attributes such as color, size, and leaf morphology, allowing for highly reliable diagnoses of plant physiological conditions and the detection of potential developmental anomalies.

In this study, the selected crop is Stevia (Stevia rebaudiana Bertoni), a plant widely recognized for its leaves' high content of steviol glycosides (SG). These compounds serve as natural, calorie-free sweeteners and are safe for consumption by both children and adults. Native to South America, this species is now cultivated in various regions worldwide due to its remarkable adaptability to different climatic conditions, attributed to its high genetic variability. In its natural environment, it grows as a perennial plant; however, in colder climates, it behaves as an annual species. Genetic improvement efforts for Stevia focus on developing varieties with increased biomass production, resistance to environmental changes, and, most importantly, higher concentrations of secondary metabolites [16].

From a technological perspective, the most valuable compounds in Stevia rebaudiana are SGs, which are responsible for its characteristic sweetness. These include stevioside, rebaudiosides A, B, C, D, E, and F, dulcoside A, and steviolbioside. According to [17], the most common SGs are stevioside and rebaudiosides A and C, while the others are present in significantly lower concentrations.

The production process of Stevia begins with the selection and planting of seeds or seedlings in soils that meet the optimal edaphoclimatic conditions for its development. Throughout its growth cycle, the plant requires a balanced nutrient supply and continuous soil pH monitoring to prevent mineral deficiencies or toxicities that could compromise its growth [18].

One of the main Stevia producers in Colima, Mexico is Rancho Tajeli (19.2370789, -103.6769232), a family owned business founded in 2015 in the municipality of Cuauhtémoc (Figure 1). Specializing in both soil and greenhouse cultivation, this company benefits from optimal agroclimatic conditions.

As plants reach physiological maturity, their leaves are harvested, serving as the primary source of SG, the compounds responsible for their characteristic sweetness. The harvested leaves are then subjected to a drying process, which can be carried out through natural sun drying or using industrial dryers, depending on environmental conditions and available infrastructure. After dehydration, the dried leaves undergo extraction and purification processes, yielding refined SG concentrations in crystal or powder form, which are later used as natural sweeteners in the food industry [19].

To ensure efficient Stevia production, optimizing soil conditions is crucial, as the hydrogen potential (pH) plays a fundamental role in the availability of essential nutrients. The presence of micronutrients such as iron, zinc, magnesium, and boron is critical for various physiological functions of the plant, including photosynthesis and the synthesis of secondary metabolites. However, the availability of these elements is directly influenced by soil pH. Values outside the optimal range can alter nutrient absorption, leading to adverse effects on plant development and SG production [20].

In acidic soils (below pH 5.5), reduced calcium and magnesium absorption has been reported,

Table 1. Related works

Reference	Crop	Methodology	Accuracy Results	Observations
[25]	Cob	CV and deep learning for disease detection	92%	Uses drone images to monitor crop health in real time.
[26]	Wheat	ANN for yield prediction	88%	Focused on optimizing water use through moisture sensors.
[27]	Potato	Disease classification using ANN	95%	Combines multispectral images with convolutional ANNs.
[28]	Tomato	Nutrient deficiency detection with CV	90%	The system identifies leaf color changes to predict nutrient issues.
[29]	Soybean	CV and ANN for growth monitoring	93%	Uses high resolution cameras to capture detailed images of plant growth.

leading to nutrient deficiency symptoms such as leaf yellowing due to iron chlorosis . Additionally, soil acidity can cause aluminum and manganese toxicity, directly affecting plant physiology and reducing yield. In contrast, in alkaline soils (above pH 7.5), the absorption of micronutrients such as iron and zinc can be severely impaired, limiting chlorophyll biosynthesis and, consequently, Stevia's vegetative development. These conditions can visually manifest as brownish tones or necrosis along leaf margins, indicating critical nutrient deficiencies that compromise crop quality and productivity [20].

Given the impact of soil pH on Stevia physiology and its production of sweetening compounds, developing technological tools for continuous monitoring is essential. In this context, AI and CV applications represent an innovative and efficient alternative for classifying and predicting soil pH levels in agricultural settings. The combination of advanced image processing techniques with ANN models enables the identification of leaf coloration patterns and their correlation with pH values, facilitating the implementation of data driven agronomic strategies [21].

The integration of CV and ANN in agriculture represents an innovative solution to optimize resource use, enhance sustainability, and address current challenges in agricultural production. This approach not only enables the monitoring of key parameters such as soil pH and leaf physical characteristics but also facilitates the automatic classification of Stevia crop health into acidic, optimal, and alkaline categories. By leveraging this technology, crop quality is improved by detecting and correcting issues before they negatively impact production, providing valuable information to maximize yield and ensure the sustainability of a globally significant crop.

The hypothesis proposed in this study is that the combination of CV and ANN will allow for high precision classification of soil pH levels using statistically significant metrics to evaluate model performance. These metrics include Matthews Correlation Coefficient (MCC), which provides a balanced measure of classifier performance, as well as accuracy, recall, and F1-score, offering a more comprehensive analysis of the system's effectiveness. To further validate the model, a Hold-Out method is applied, where the dataset is split into training and testing subsets to assess generalization performance and avoid overfitting [22, 23, 24].

Several studies exploring the use of advanced technologies in agriculture have been reviewed, and their results are presented in Table 1. These studies highlight the application of AI tools for resource optimization and agricultural productivity enhancement, reinforcing AI’s role in the digital transformation of the agrifood sector

Finally, it is important to highlight that the previous studies presented in Table 1 have achieved significant results in various applications of AI in agriculture. However, none of them have specifically focused on evaluating soil pH in Stevia crops using ANN and CV. This gap in the literature underscores the relevance and novelty of the present research, which proposes an innovative solution for soil pH monitoring in Stevia cultivation using ANN and CV.

This comprehensive approach not only optimizes Stevia production but also provides advanced technological tools to farmers, enabling them to address the challenges of modern agriculture with greater precision and efficiency. The system's ability to generate accurate

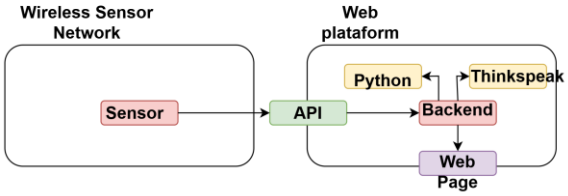

Fig. 2. Proposed solution

Table 2. Key parameter

Parameter	Acidic	Optimal	Alkaline
pH	<5.5	5.5-7.5	>7.5

predictions minimizes the risks associated with soil condition fluctuations, maximizing economic, social, and environmental benefits.

2. Materials and Methodology

The proposed solution, as shown in Figure 2, utilizes a Wi-Fi hydroponics kit [30] to automate the monitoring and control of hydroponic systems through the ThingSpeak cloud platform. The kit collects data from sensors measuring temperature, pH, electrical conductivity, and nutrient levels essential for optimal plant growth.

The collected data serves as input for the Neural Network (NN), which, during training, adjusts its parameters using optimization algorithms to minimize prediction errors. After training, the model is evaluated using validation data, and parameters are fine tuned as needed to improve accuracy and ensure reliable predictions. This device enables precise soil pH measurement, a critical factor for optimizing plant development.

The data collected by the sensor serves as input for training an ANN, which adjusts its parameters through optimization algorithms to minimize prediction errors. The model is then validated using an independent dataset, refining its parameters as necessary to enhance accuracy and ensure reliable predictions.

2.1 Key Parameter

Soil pH was selected as the primary parameter for assessing Stevia health due to its direct impact on the availability of essential nutrients. According to [5], an optimal pH range of 5.5 to 7.0 maintains a balanced nutrient supply, promoting healthy plant development.

Values outside this range can compromise nutrient absorption, affecting SG production and, consequently, crop quality:

- Acidic soils (pH < 5.5): Cause iron and magnesium deficiency, leading to leaf chlorosis (yellowing) and reduced photosynthesis.
- Alkaline soils (pH > 7.5): Promote toxic accumulation of salts and micronutrients, potentially causing leaf necrosis (brown or burnt tones) and disrupting plant metabolic processes.

These adverse effects on crop health are summarized in Table 2.

2.2 Data Acquisition

For soil pH measurement, the Atlas Scientific Wi-Fi hydroponics kit (Fig. 3) was selected, enabling remote monitoring and control of hydroponic systems. This system uses an Adafruit HUZZAH32 CPU, programmed via Arduino IDE, to upload data to ThingSpeak, a cloud platform. Its selection was based on several technological advantages, including:

- High sensitivity and accuracy in measurements.
- pH measurement range from 0 to 14 with a resolution of 0.01 pH.
- Rapid response, allowing real time data acquisition.
- Data visualization on both PC and mobile devices, ensuring efficient remote monitoring.

Compared to traditional methods and conventional sensors, this device excels in durability, reliability, and adaptability to harsh agricultural conditions. Its integration with AI and CV tools ensures the acquisition of high quality data for soil pH analysis and prediction, even in hard to reach locations such as Rancho Tajeli.

Fig. 3. Atlas Scientific Wi-Fi Hydroponics Kit

Fig. 4. Example of 4 images of Stevia plants captured with the light box

Fig. 5. Portable Lightbox

In addition to pH monitoring, images of Stevia plants were captured at Rancho Tajeli, resulting in a dataset of 200 images for further analysis (Fig. 4).

To ensure consistent lighting and standardized image size, a nikon D7500 camera was mounted inside a portable lightbox, as shown in Figure 5.

The lightbox measures 60 × 60 × 70 cm and features a 28 lux led ring light at the top, ensuring controlled illumination for image acquisition.

2.3 Image Preprocessing and Augmentation

Data preprocessing is a fundamental stage in AI model development, particularly in CV and ANN applications. This step enhances data quality and optimizes model accuracy. As noted in [31], preprocessing includes normalization, cleaning, and data transformation to minimize noise and inconsistencies.

For image analysis, advanced techniques such as rescaling, segmentation, and background removal were employed, which have proven effective in agricultural applications [32, 33, 34]. These techniques ensure that the model receives clear and consistent input, facilitating ML. According to [35], proper preprocessing in agricultural environments enhances complex pattern detection and improves classification accuracy for plant health assessment.

2.4 Extraction of Color Data in Hexadecimal Format

To extract hexadecimal color data from the captured images of Stevia plants (Fig. 6), a CV approach was implemented using the OpenCV library. This process involved converting images to the HSV (Hue, Saturation, Value) color space to facilitate the detection of the predominant green color in the leaves.

The image processing workflow consisted of the following steps:

1. Conversion to the HSV color space: This enabled more effective segmentation of the green color, following the methodology described in [36].
2. Definition of a specific color range: A threshold was established to identify green areas in the image.
3. Creation of a binary mask: Pixels within the defined range were assigned a value of 1 (white), while the rest were set to 0 (black).

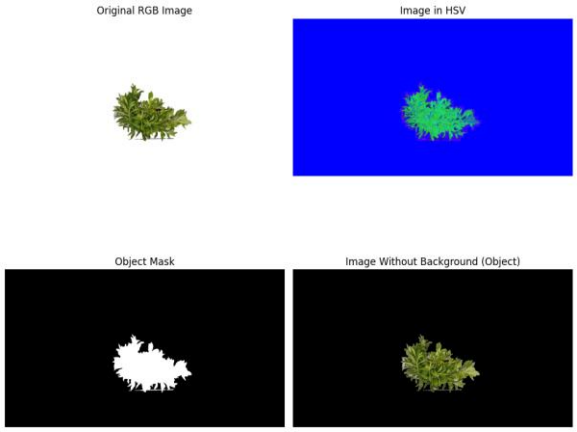

Fig. 6. Extraction of Color Data in Hexadecimal Format

4. Application of the mask to the original image: This allowed isolation of the regions of interest, corresponding to Stevia plants.
5. Contour detection: Green areas were identified by extracting contours, locating the region with the highest presence of green.
6. Centroid calculation: The central point of each contour was determined for a more precise analysis.

2.5 Data Augmentation via Rotation and Mirroring

To enhance the model's generalization capability, data augmentation techniques (Fig. 7) were applied using the Pillow library. The following strategies were implemented:

- Image Rotation: Each image was rotated in 60° increments, generating six different rotated versions of each original sample.
- Dataset Expansion: Starting from 200 original images, the rotation process produced 1,200 images (200 original × 6 rotations).
- Horizontal Mirroring: A horizontal reflection transformation was applied to each rotated image, effectively doubling the dataset size to 2,400 images (1,200 rotated images × 2, including mirrored versions). This step further enriched the dataset by capturing symmetrical variations relevant to soil pH classification.

The application of these techniques enhanced the model, allowing it to better adapt to different perspectives of Stevia plants and improve its performance in classifying the visual characteristics of the plants. To enhance the model's generalization capabilities, Gaussian noise was introduced as a data augmentation technique. This method [38] perturbs the original data by adding small variations drawn from a normal distribution with mean zero and a standard deviation of 0.02. The augmentation process was applied to all relevant features, ensuring that the generated samples retained the overall distribution characteristics while introducing slight variations that help the model learn more robust patterns. As a result, the dataset was expanded to a total of 7,590 samples through rotation, mirror, and Gaussian noise augmentation, applying a scaling factor of n to the original dataset size ($2{,}400 \times n \approx 7{,}590$). This factor reflects the additional augmentation achieved through Gaussian noise, where each image in the 2,400 image dataset was, on average, expanded by $n\text{-}1$ additional variations [37].

2.6 Conversion and Representation of Color Data

To achieve a compact representation of color information, the central pixel value of each image was selected and converted into hexadecimal format. These values were then transformed into a 24-bit binary matrix, corresponding to the RGB (Red, Green, Blue) channels [39].

This transformation enabled an efficient data structure for processing by the ANN, facilitating the classification of soil pH into three categories:

- Acidic,
- Optimal,
- Alkaline.

By applying this approach, the model's prediction accuracy for Stevia crop health was optimized, ensuring a reliable classification based on leaf color analysis.

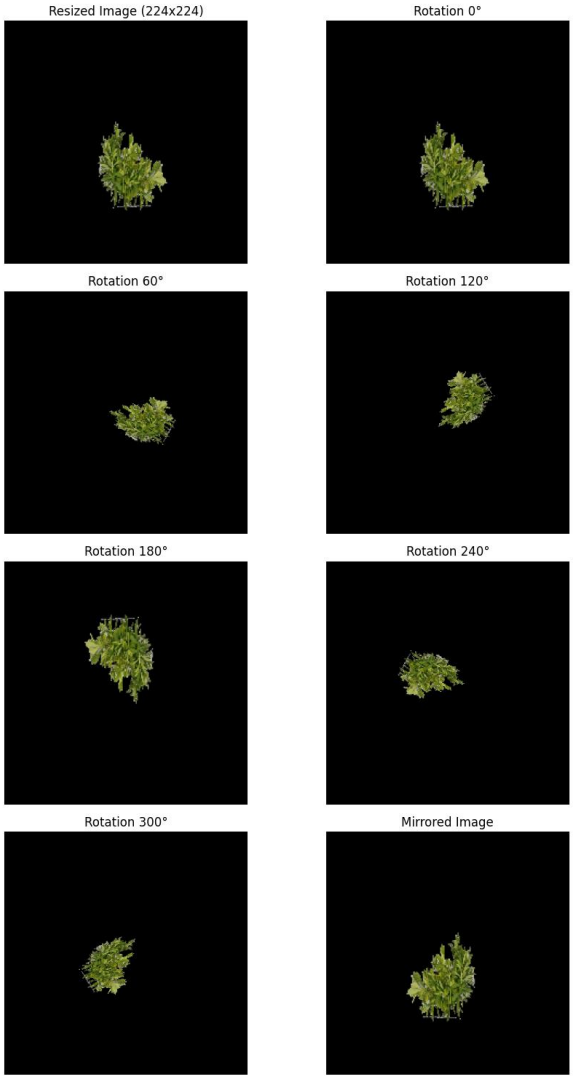

Fig. 7. Data Augmentation via Rotation and Mirroring

2.7 Evaluation Metrics

To assess the model's performance, it is essential to select appropriate metrics that enable an objective interpretation and comparison of results.

As stated in [40], classification models are typically evaluated using the following metrics: Precision, Recall (Sensitivity), F1-score and Accuracy. These metrics, defined in Equations (1) to (4), provide a comprehensive analysis of the model's classification performance.

2.7.1. Precision

Precision (Eq. 1) is defined as the proportion of correct positive predictions among all instances identified as positive by the model.

This metric evaluates the accuracy of positive predictions, which is particularly important in applications where false positives can have a significant impact, such as disease diagnosis and fraud detection [41]:

$$\text{Precision (P)} = \frac{TP}{TP+FP}, \tag{1}$$

where:

- *TP (True Positives)*: Correctly predicted positive cases.
- *FP (False Positives)*: Incorrectly predicted positive cases.

2.7.2. Recall (Sensitivity)

Recall (Eq. 2), also known as sensitivity or the true positive rate, evaluates the proportion of actual positive instances that were correctly identified by the model. This metric is crucial in scenarios where false negatives can have severe consequences, such as in security systems or disease detection [42].

$$\text{Recall (R)} = \frac{TP}{TP+FN}, \tag{2}$$

where:

- *FN (False Negatives)*: Incorrectly predicted negative cases.

2.7.3. F1-Score

The F1-score (Eq. 3) is the harmonic mean of precision and recall. It is especially useful when class imbalance exists, as it provides a balance between both metrics [43]:

$$\text{F1} - \text{score} = 2 * \frac{P * R}{P+R}, \tag{3}$$

Table 3. Confusion Matrix

	Predicted Values	
Actual values	TN	FN
	FP	TP

This indicator is valuable in applications where neither precision nor recall alone can be prioritized, but rather a balance between both is required.

2.7.4. Accuracy

Accuracy (Eq. 4) measures the overall proportion of correct predictions relative to the total number of analyzed instances. This metric is useful when classes are balanced, but it can be misleading in cases with class imbalances [44]:

$$\text{Accuracy} = \frac{TP + TN}{TP + TN + FP + FN}, \quad (4)$$

where:

- *TN (True Negatives)*: Correctly predicted negative cases.

2.7.5. Confusion Matrix

These metrics (precision, recall, f1-score and accuracy) are derived from the confusion matrix (Table 3), which categorizes the model's predictions into four main groups:

1. *True Positives (TP)*: Correctly identified positive cases.
2. *False Positives (FP)*: Negative cases incorrectly classified as positive.
3. *True Negatives (TN)*: Correctly identified negative cases.
4. *False Negatives (FN)*: Positive cases incorrectly classified as negative.

The confusion matrix provides a detailed summary of the model's performance on a test dataset with known real labels [45]. Its analysis allows for an interpretation of prediction distribution, identifying how often the model classifies correctly and where errors occur. This tool is essential in classification model evaluation, as it enhances the understanding of prediction quality and helps detect potential biases in the model.

Evaluation metrics derived from the confusion matrix have been widely implemented in CV and ANN classification studies. Precision and recall were leveraged to evaluate an agricultural disease classification system [46], the F1-score was applied to benchmark the effectiveness of different ANN architectures for medical image classification [47], and accuracy was employed to assess object detection models in aerial images [48].

2.7.6. Matthews Correlation Coefficient

Additionally, MCC, defined in Equation (5), is employed as a complementary metric to evaluate model performance. According to [49], MCC is a statistically reliable metric that provides a balanced assessment of model quality.

This formula extends the MCC for multiclass classification by incorporating information from all confusion matrix elements (Table 4), providing a balanced evaluation even in the presence of class imbalances.

$$MCC = \frac{\sum k \sum l \sum m Ckk Clm - Ckl Cmk}{\sqrt{\sum k (\sum l Ckl)(\sum m, m = kCkm) \cdot \sum k (\sum l Clk)(\sum m, m = kCmk)}}, \quad (5)$$

where:

- *Ckk* represents the diagonal elements of the confusion matrix (correctly classified instances for each class).
- *Ckl* and *Clk* represents the misclassified instances, where class k was predicted as class l.
- *Clm* and *Cmk* represent other off diagonal misclassifications.

Unlike traditional metrics such as precision or accuracy, MCC accounts for class distribution in the dataset, making it particularly useful in scenarios with imbalanced classes.

- An MCC close to +1 indicates a highly accurate model.
- An MCC of 0 suggests random classification performance.

Table 4. Confusion matrix used in MCC formula for multiclass classification

	Predicted A	Predicted B	Predicted C
Actual A	Ckk	Ckl	Ckm
Actual B	Clk	Ckk	Clm
Actual C	Cmk	Cml	Ckk

- An MCC of -1 reflects completely incorrect classification, indicating a poorly performing model.

By incorporating MCC into the model evaluation, a more precise and objective interpretation of overall performance is achieved. This ensures that the ANN not only classifies most cases correctly but also maintains a balanced performance across all categories in the analyzed problem.

2.8 ANN Architecture

The hyperparameters of the ANN were optimized using Particle Swarm Optimization (PSO) to determine the best configuration of layers, neurons, dropout rate, and activation function. Inspired by the collective behavior of swarms in nature, PSO iteratively adjusts candidate solutions based on their individual best positions (*pbest*) and the global best position (*gbest*), allowing for an efficient exploration of the hyperparameter space.

This optimization process enhances convergence towards an optimal ANN architecture by balancing exploration and exploitation, reducing computational costs compared to exhaustive search methods. The effectiveness of PSO in optimizing neural networks has been demonstrated in various domains, including network security, power distribution, and intelligent transportation systems, where it has outperformed traditional tuning approaches in terms of accuracy and computational efficiency [50,51,52].

The optimization process (Table 5) allowed us to find the best combination of hyperparameters, resulting in an efficient and high-performance ANN, as demonstrated in previous studies on similar applications.

2.8.1 Layers and Neurons

The model architecture begins with an input layer, which receives the previously normalized features using StandardScaler. This normalization process ensures that each variable has a mean of 0 and a standard deviation of 1, facilitating training and preventing scaling issues in input values. This approach enhances generalization capability and improves classification accuracy, as demonstrated in previous studies on similar applications [53, 54, 55].

The hidden layers consist of three levels with 270 neurons. Each of these layers uses the Rectified Linear Unit (ReLU) activation function, widely recognized for its ability to handle non linearity and mitigate the vanishing gradient problem, promoting deep learning in the model.

To enhance training stability and efficiency, Batch Normalization is applied after each hidden layer, a technique that reduces internal covariate shift and accelerates model convergence. Additionally, Dropout with a 30% rate is incorporated, preventing overfitting by randomly deactivating certain neurons during training, ensuring better generalization to unseen data.

Finally, the output layer consists of three neurons, corresponding to each classification category (acidic, optimal, and alkaline). This layer employs the softmax activation function, which assigns a probability to each class, allowing the model to select the category with the highest confidence.

2.8.2 Training

The model is trained using the Adam optimizer, an algorithm that combines the advantages of Momentum and RMSprop, providing stability and fast convergence. This technique has proven to be efficient in multiclass classification tasks, making it suitable for this study [56,57].

The model was trained for 100 epochs, iteratively refining its weights to minimize the sparse categorical cross-entropy loss function. This function is particularly suitable for multiclass classification as it efficiently processes integer-encoded labels [58].

Table 5. PSO for Neural Network Hyperparameter Tuning

Algorithm: PSO for Neural Network Hyperparameter Tuning
Input: Number of particles (*n_particles* = 10), search space boundaries (*bounds*), max iterations (*iters* = 5). **Search Space Boundaries:** Hidden layers (1-5), neurons (64-512), dropout rate (0.1-0.5), activation function (ReLU or Tanh), optimizer (Adam, SGD, RMSProp, Adadelta, Adagrad), epochs (50, 100, 150). **1. Initialization:** Set swarm with random values within the defined *bounds*. **2. Iterative Optimization:** Repeat for *iters* iterations: - Evaluate each particle's position by training and testing an ANN with the selected hyperparameters. - Update personal best (*pbest*) if the new position yields a better performance. - Update global best (*gbest*) among all particles. - Adjust velocity and position using PSO Equation (6): *v = w*v + c1 * r1 * (pbest - xid) + c2 * r2 * (gbest - xid)* (6) where: – *v* is the velocity of the particle in dimension d. – *xid* is the position of the particle – *w* is the inertia weight, which controls the influence of the previous movement. – *c1* and *c2* are the learning coefficients that regulate the influence of pbest and gbest. – *r1,r2* are random numbers in the range [0,1], introducing randomness in the exploration process. After updating velocity, the position update follows: **position = position + velocity** **3. Convergence:** After iterations, return the *gbest* hyperparameters with the best model performance. **4. Optimal Configuration:** The best ANN configuration found: - Number of hidden layers = 3 - Number of neurons per layer = 270 neurons - Dropout rate = 30% - Activation function = ReLU for hidden layers, Softmax for the output layer - Optimizer = Adam - Number of epochs = 100

2.8.3 Performance Evaluation

To assess the model's effectiveness, the Hold-Out methodology was implemented, a widely used supervised learning approach. The dataset, consisting of 7,590 samples, was generated using 200 original images and enhanced through data augmentation techniques including rotation, mirroring, and Gaussian noise addition as mentioned in section *2.5 Data argumentation via rotation and mirroring*. This ensures that the training set is robust and diverse, without altering the real distribution of the data. The final dataset consists of a combination of original and synthetically generated images. The data was split as follows:

- 80% for the training set (6,072 samples): Implemented to optimize model weights and improve generalization.
- 20% for the validation set (1,518 samples): Implemented to evaluate model performance on unseen data and prevent overfitting**.**

To measure the model's effectiveness, key evaluation metrics were employed to assess its predictive capability:

- Accuracy: Reflects the percentage of correct predictions over the total number of evaluated samples.
- MCC: Evaluates class balance, particularly useful in scenarios with imbalanced classes.

The ANN architecture summarized in Table 6 provides an overview of the proposed model.

Table 6. StePHVIA Neural Network Model Algorithm

Algorithm: Neural Network Model for pH Classification in Stevia Crops
Input: Training data $X_{train} \in R^{n\times3}$(RGB feature values), labels $y_{train} \in \{0, 1, 2\}$ (pH categories: acidic, optimal, alkaline), learning rate α, number of epochs e,batch size s. **Output:** Trained neural network model and evaluation metrics (accuracy and MCC). **1. Initialization:** Define the sequential architecture - First hidden layer with 270 neurons, weights $W_1 \in R^{270\times3}$, biases $b_1 \in R^{270}$ Batch Normalization, ReLU activation, and Dropout (30%). - Second hidden layer with 270 neurons, weights $W_2 \in R^{270\times270}$, biases $b_1 \in R^{270}$ Batch Normalization, ReLU activation, and Dropout (30%). - Third hidden layer with 270 neurons, weights $W_3 \in R^{270\times270}$, biases $b_1 \in R^{270}$ Batch Normalization, ReLU activation, and Dropout (30%). -Output layer with 3 neurons, weights $W_o \in R^{3\times270}$, biases $b_o \in R^3$, and softmax activation function. **2. Training:** For each epoch i from 1 to e=*100*: - Shuffle X_{train} y and y_{train}. Divide into batches of size s. For each batch: 1. Compute forward propagation: $Z_1 = W_1X + b_1$, A_1 = ReLU(BatchNorm(Z_1)). $Z_2 = W_2A_1 + b_2$, A_2 = ReLU(BatchNorm(Z_2)). $Z_3 = W_3A_2 + b_3$, A_3 = ReLU(BatchNorm(Z_3)). $Z_o = W_oA_3 + b_o$, A_o = softmax(Z_o). 2. Compute the loss L using sparse categorical crossentropy *sparse categorical crossentropy*: $L = -\frac{1}{s}\sum_{i=1}^{s}\sum_{j=1}^{3} y_{ij}\log(A_{oj})$. 3. Backpropagation and parameter update using Adam. **4. Validation:** Evaluate on X_{val} to obtain: -Accuracy (Eq. 4) - Matthews Correlation Coefficient (Eq. 5)

3 Results

As part of the results analysis, a Comma Separated Values (CSV) file was generated using images captured from Stevia plants at Rancho Tajeli and pH values obtained through a portable soil detector. The dataset consists of 200 images, classified into three categories: optimal, acidic, and alkaline.

Additionally, descriptive statistics, such as mean, median, mode, and standard deviation, were computed to evaluate the distribution and variability of the recorded soil pH values.

3.1 Statistical Analysis of Soil pH

According to the results presented in Table 7, the analyzed soils exhibit a predominantly optimal pH, with a slight tendency toward acidity. The median and mode, both with a value of 6.36, indicate that most values cluster around this range, suggesting that this value is representative of the predominant soil conditions in the evaluated fields.

However, the standard deviation of 1.55 reveals a significant dispersion in the values, indicating the presence of both acidic and alkaline conditions in different cultivation areas. This variability highlights the importance of implementing monitoring and adjustment strategies to ensure optimal growth conditions for Stevia.

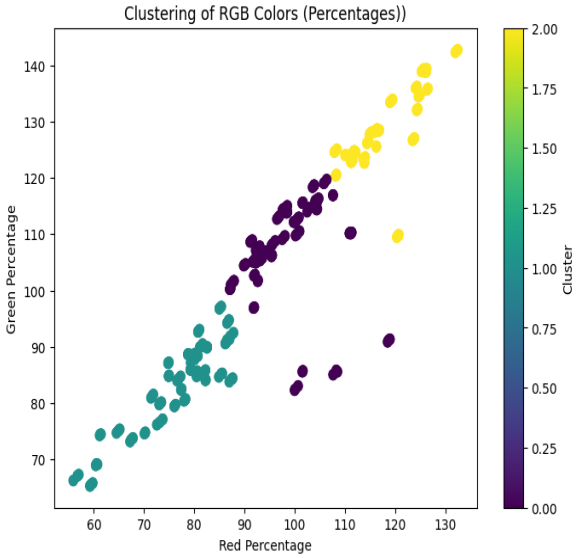

Fig. 8 . Clustering of RGB Colors (Percentages)

Table 7. Statistical measuring

Statistical Measuring	Value
Mean	6.09
Median	6.36
Mode	6.36
Standard Deviation	1.55

3.2 RGB Color Extraction and Processing

The generated CSV file also contains the RGB color percentages for each image, along with the average of these values in hexadecimal format. This data allows the ANN to process and adjust its weights effectively.

For each image, the system calculates the percentage of each color channel RGB relative to the total number of pixels in the image. These values are then converted into hexadecimal codes, facilitating interpretation and processing within the ANN.

Finally, the program stores the image name, RGB channel values, and their hexadecimal representation in the CSV file.

3.3 Category Labeling: Acidic, Optimal, and Alkaline

To classify the leaf samples based on their RGB characteristics, the K-means clustering algorithm was applied. This unsupervised machine learning technique partitions data into k clusters by minimizing intra-cluster variance. K-means is efficient, easy to implement, and interpretable, making it suitable for tasks like this where data is unlabelled [59]. It works well with numerical and continuous features like RGB values and ensures that each cluster represents a homogeneous group of similar data. In this study, three clusters were defined, each representing a different category of soil pH based on leaf coloration.

After obtaining the RGB values and converting them into hexadecimal codes, the samples were classified into three distinct categories: acidic, optimal, and alkaline (Fig. 8). This categorization is based on the dominant color components in each cluster:

- Acidic Category: Characterized by a dominance of the red (R) and green (G) channels, leading to yellowish tones. The mean RGB values recorded for these samples were (98.99, 107.50, 51.39).
- Alkaline Category: Exhibited lower intensity of the red (R) and green (G) channels, resulting in brownish or burnt tones, which may indicate nutrient deficiencies or salt accumulation. The mean RGB values for this category were (76.44, 83.12, 43.57).
- Optimal Category: Defined by the highest intensity in the green (G) and red (R) channels, suggesting a healthy green color in the leaves. The mean RGB values recorded for this category were (117.52, 128.29, 63.80).

These results establish a correlation between leaf colorimetry and soil pH, providing a key input for the development of AI based models aimed at automatically classifying the health status of Stevia crops.

3.4 Training Results of the StePHVIA Model

Figures 9 and 10 presents the evolution of accuracy and loss over the 100 training epochs of

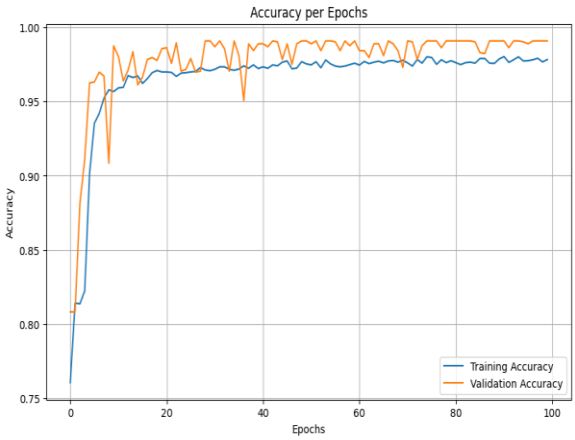

Fig. 9 . Accuracy per Epochs

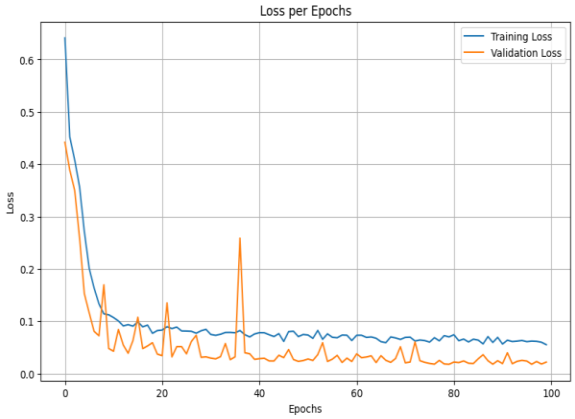

Fig. 10 . Loss per Epochs

the StePHVIA model. A stable trend and a progressive improvement in performance were observed in both the training and validation datasets.

3.4.1 Accuracy per Epoch

The evolution of accuracy during training is illustrated in Figure 9. A rapid increase is evident in the first 20 epochs, followed by stabilization around 99%. Validation accuracy follows a similar pattern, remaining slightly below training accuracy, indicating that the model generalizes well with no significant signs of overfitting.

3.4.2 Loss per Epoch

As shown in Figure 10, the loss function behavior is observed throughout training. In the initial iterations, a sharp decrease in training loss is observed, converging to a value close to 0.0185 in the final epochs. Validation loss, despite initial fluctuations, follows a downward trend, staying close to training loss, confirming the model's stability.

These results indicate that StePHVIA has achieved optimal performance, with 99% accuracy and low loss, demonstrating a high capacity to correctly classify the soil pH status in Stevia crops. The stability of the metrics and the convergence of training and validation values further reinforce the model's reliability in classification tasks.

3.5 Confusion Matrix Results

As demonstrated in Figure 11 presents the confusion matrix obtained during the evaluation of the StePHVIA model, providing a detailed representation of the model's performance in classifying soil pH into three categories: acidic, optimal, and alkaline.

Each cell in the matrix indicates the number of predictions made for each category in comparison with the actual values. The results show that the model exhibits a high level of accuracy, with predominant values along the main diagonal, indicating correct classification in most cases.

- The first row shows that the model correctly classified 477 samples of optimal soils with no errors.
- The second row indicates that out of 531 acidic soil samples, 528 were classified correctly, while 2 were misclassified as optimal and 1 as alkaline.
- The third row reveals that the model correctly identified 495 alkaline soil samples, with a small number of errors, 15 were misclassified as acidic.

The model's performance in classifying optimal soils was perfect (100%), while errors in the acidic and alkaline categories were minimal, demonstrating a robust discrimination capability.

ISSN 2007-9737

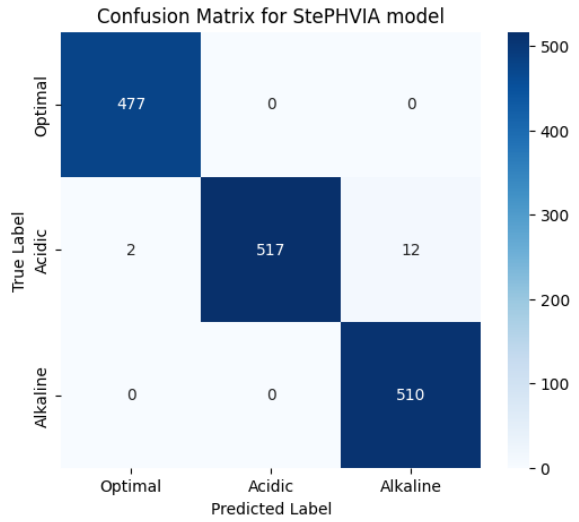

Fig 11. Confusion Matrix for StePHVIA model

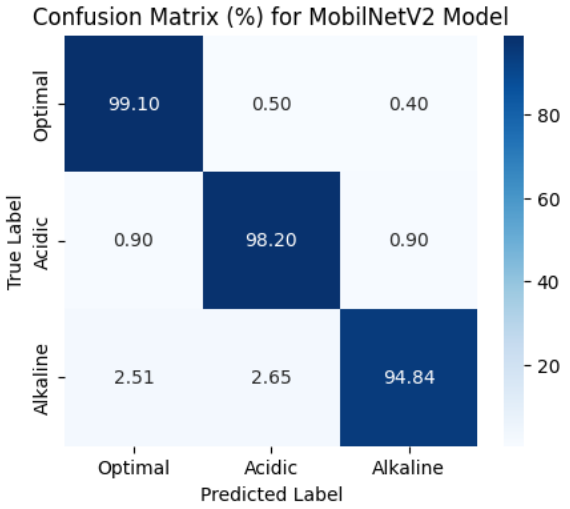

Fig. 12. Confusion Matrix (%) for MobilNetV2 model

3.6 Model Comparison: MobileNetV2 vs. ResNet-50 vs. StePHVIA

To evaluate the performance of the proposed StePHVIA model, a comparison was conducted with two pretrained neural network architectures: MobileNetV2 and ResNet-50. These models were selected based on their distinctive characteristics and applicability to image classification tasks under different computational constraints. All models were trained using the same dataset and under similar conditions to ensure a fair evaluation.

3.6.1 MobileNetV2

MobileNetV2 [60] is a convolutional neural network (CNN) optimized for mobile devices and environments with hardware constraints. It utilizes depthwise separable convolutions and inverted residual blocks, which significantly reduce the number of parameters and computational cost without compromising accuracy.

MobileNetV2 results:

- Validation Accuracy: 97.38%
- Validation Loss: 0.0199
- MCC: 0.97
- Metric Report:
  - Macro Average Precision: 97%
  - Macro Average Recall: 98%
  - Macro Average F1-score: 97%

MobileNetV2 demonstrated a good balance between precision and recall (Fig. 12), performing particularly well in the alkaline category, where it showed strong reliability in identifying this class with high precision and recall.

3.6.2 ResNet-50

ResNet-50 [61] is a 50 layer deep convolutional neural network based on residual blocks. Its architecture allows for training deeper networks without suffering from the vanishing gradient problem. However, due to its high complexity, it requires more data and greater computational power for optimal performance.

ResNet-50 results:

- Validation Accuracy: 76.38%
- Validation Loss: 0.58
- MCC: 0.65
- Metric Report:
  - Macro Average Precision: 76%
  - Macro Average Recall: 74%
  - Macro Average F1-score: 75%

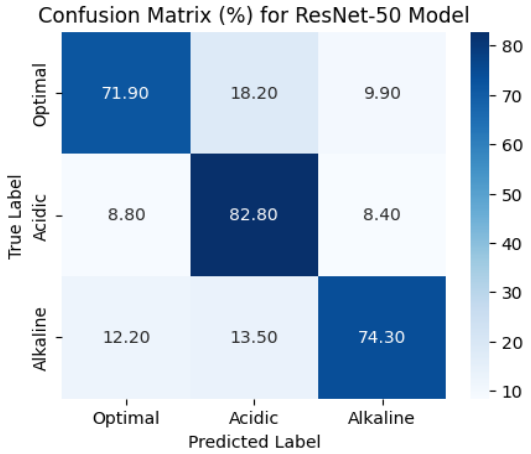

Fig 13. Confusion Matrix (%) for ResNet-50 model

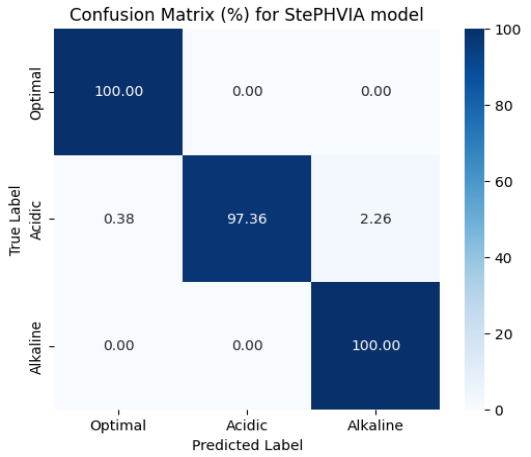

Fig. 14. Confusion Matrix (%) for StePHVIA model

ResNet-50 exhibited lower performance compared to MobileNetV2 (Fig. 13). Its metrics indicate generalization issues, with a reduced ability to distinguish between pH classes. The fluctuation in accuracy and recall suggests that the model may have overfitted the training data, failing to generalize effectively to unseen data.

3.6.3 StePHVIA

StePHVIA is a hybrid model that combines CV and an ANN. Instead of using convolutions to extract features, StePHVIA directly utilizes RGB values from Stevia plants and a supervised deep learning approach with augmented data.

StePHVIA Results:

- Validation Accuracy: 99%
- Validation Loss: 0.0185
- MCC: 0.9823
- Metric Report:
  - Macro Average Precision: 99%
  - Macro Average Recall: 99%
  - Macro Average F1-score: 99%

The StePHVIA model demonstrated strong classification performance (Fig. 14), achieving high precision and recall across all categories. Notably, it performed exceptionally well in the Optimal and Alkaline categories, with 100% accuracy in both, while maintaining a high reliability in identifying the Acidic class.

StePHVIA demonstrated exceptional performance, significantly surpassing MobileNetV2 and ResNet-50 in key evaluation metrics such as accuracy, recall, and the MCC. This model's combination of CV techniques and ANN proved to be a powerful approach, enabling it to accurately classify soil pH levels with remarkable precision.

The model's validation accuracy of 98.91% and recall of 99% reflect its ability to correctly identify the majority of relevant samples. Most notably, StePHVIA achieved an MCC of 0.9823, which underscores the model's high classification reliability. The MCC score, in particular, demonstrates that the model not only has high accuracy but also robust performance in distinguishing between the different classes, even in the case of imbalanced data. This exceptional performance is clearly shown in Table 8, highlighting StePHVIA's superior classification capabilities compared to other architectures.

In addition to its strong classification performance, StePHVIA also demonstrates remarkable computational efficiency. These results confirm the effectiveness of ANN and CV in PA, providing a real time and low cost alternative for soil monitoring. Additionally, the comparison of training times highlights the model's efficiency: while StePHVIA required only 50 seconds,

Table 8. Comparison of the resutls

Model	Validation Accuracy(%)	Recall (%)	F1-Score(%)	Validation Loss	MCC	Training Time
MobileNetV2	97.38	97.00	97.00	0.0199	0.9722	2h 17m
ResNet-50	76.38	74.00	75.00	0.058	0.65	6h 48m
StePHVIA	**98.81**	**99.00**	**99.00**	**0.0185**	**0.9823**	**50s**

pretrained CNNs such as MobileNetV2 and ResNet-50 required 5 hours 35 minutes and 6 hours 48 minutes, espectively. This significant reduction in computational cost makes StePHVIA a practical and scalable solution for resource limited environments.

The tests were performed on a Central Processing Unit (CPU) with the following technical specifications:

- Operating System: Windows 11
- Host: Alienware Aurora R7
- Processor: Intel Core i7-8700
- RAM: 16 GB

3.7 Web Application

Additionally, a web application (Fig. 15) was implemented and hosted on a local server to facilitate the uploading and prediction of Stevia plant images. This tool provides an intuitive and accessible interface, allowing users to upload images of Stevia plants directly from their devices. The application processes these images using the previously trained NN model, classifies pH levels into acidic, optimal, and alkaline, and presents the results in a clear and visual manner.

The functionality of this platform includes the automatic management of uploaded images, which are stored in a dedicated directory for further analysis. Furthermore, the application is scalable and can be deployed on a remote server in the future, expanding its reach and usefulness for farmers and other stakeholders interested in the evaluation of Stevia crops.

4 Conclusions

These results demonstrate the potential of the system as a practical and accurate tool for the continuous monitoring of soil health and Stevia plants. Its implementation enables farmers to quickly identify problematic areas, optimizing the use of fertilizers and soil amendments, and promoting a more efficient crop management strategy.

In combination with ANN and CV, this model represents a significant advancement in PA, enabling data driven decision making and enhancing the productivity and sustainability of Stevia crops.

The developed system not only reduces reliance on manual and costly methods, which are typically slower and less accurate, but also facilitates real time informed decision making. This significantly contributes to improving crop productivity and sustainability by providing precise data on soil pH status and Stevia plant health.

The integration of ANN and CV enables a PA approach, enhancing farm management efficiency and supporting high quality production. StePHVIA stands out as an innovative tool, promoting sustainable and optimized farming practices.

5 Discussion and Future Work

The StePHVIA model demonstrated high reliability in classifying Stevia soil pH, outperforming MobileNetV2 and ResNet-50 with 98.81% accuracy and an MCC of 0.9823. Its RGB based approach proved computationally efficient, while augmentation techniques enhanced model generalization. However, further validation is needed, as the dataset was collected under controlled conditions. External factors like leaf damage, pests, and water stress could impact classification accuracy, requiring improved preprocessing techniques.

To enhance scalability, future research will expand the dataset with images from diverse soil types and climates, incorporating field trials, to validate real-world performance. Addressing these aspects will establish StePHVIA as a key tool in

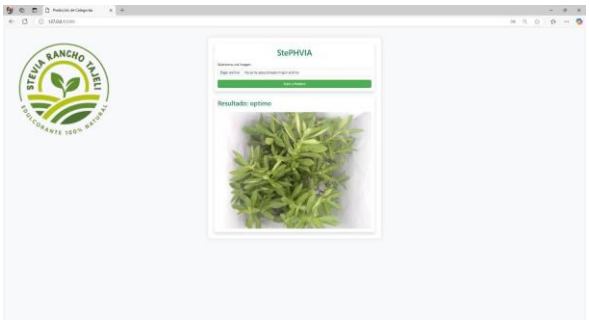

Fig 15. Web application

precision agriculture, enhancing efficiency and sustainability in Stevia cultivation.

Acknowledgements

The authors sincerely appreciate the administrative and technical support provided by SECIHTI and TecNM. Furthermore, we extend special thanks to Rancho Tajeli for allowing the implementation of the monitoring system in their stevia crops.

References

1. **Q. Xu, M. Pang, Q. Peng, J. Li, and Y. Jiang (2024).** "Application of supercritical carbon dioxide in the preparation of biodegradable polylactide membranes," Journal of Applied Polymer Science, vol. 94, no. 5, pp. 2158-2163, doi: https://doi.org/10.1002/app.21132
2. **S. Y. Liu (2020)**, "Artificial Intelligence (AI) in Agriculture," in IT Professional, vol. 22, no. 3, pp. 14-15, 1 May-June, doi: 10.1109/MITP.2020.2986121.
3. **A. González Alan (2013),** "Aplicación de la inteligencia artificial en el diseño de una antena PIFA para redes 5G," Antena, no. 167, pp. 34-41, 2021. [En línea]. Disponible: /https://www.revistaciencia.amc.edu.mx/images/revista/64_4/PDF/InteligenciaMecanica.pdf [Accedido: 27-sept.-2024].
4. **Alloghani, M.A. (2024).** AI for Sustainable Agriculture: A Systematic Review. In: Artificial Intelligence and Sustainability. Signals and Communication Technology. Springer, Cham. https://doi.org/10.1007/978-3-031-45214-7_3
5. **Oluwafunmi Adijat Elufioye, Chinedu Ugochukwu Ike, Olubusola Odeyemi, Favour Oluwadamilare Usman, & Noluthando Zamanjomane Mhlongo (2024).** AI-Driven Predictive Analytics in Agricultural Supply Chains: A Review: Assessing the Benefits and Challenges of AI in Forecasting Demand and Optimizing Supply in Agriculture. Computer Science & IT Research Journal, 5(2), 473-497. https://doi.org/10.51594/csitrj.v5i2.817.
6. **S. Haykin (2009),** Neural Networks and Learning Machines, 3rd ed. Pearson.
7. **A. Kamilaris and F. X. Prenafeta-Boldú (2018)**, "Deep learning in agriculture: A survey," Computers and Electronics in Agriculture, vol. 147, pp. 70–90, Apr. 2018.
8. **J. S. Russel and J. S. Rout (2019)**, "Applications of artificial neural networks for agricultural field monitoring and crop disease detection: A review," Agriculture Journal, vol. 63, pp. 56-68.
9. **I. L. Tsouros, S. Bibi, and P. Sarigiannidis (2019)**, "A review on UAV-based applications for precision agriculture," Information, vol. 10, no. 11, pp. 349.
10. **G. Shilpa and M. R. Meshram (2015)**, "Neural network based irrigation system for precision agriculture," International Journal of Computer Applications, vol. 116, no. 19, pp. 1-5.
11. **X. Shi et al (2020)**., "Optimizing fertilizer use in precision agriculture: A case study using deep neural networks," IEEE Transactions on Automation Science and Engineering, vol. 17, no. 3, pp. 1219-1227.
12. **L. Zhang, H. Guo, and X. Huang (2021)**, "Applications of computer vision and artificial intelligence in agriculture," Precision Agriculture, vol. 22, no. 4, pp. 1-18.
13. **A. Tripathi, S. R. Lohumi, and H. K. Choudhary (2020)**, "Computer vision based disease detection in agriculture: A review," International Journal of Applied Engineering Research, vol. 12, no. 3, pp. 445-456.
14. **J. Qiu, L. Tang, M. Z. Hasanuzzaman, and P. K. Zhang (2020)**, "A survey on computer

vision technologies for plant health monitoring," Journal of Agricultural Informatics, vol. 10, no. 3, pp. 52-66.

15. **S. R. Dubey, N. Singh, and S. K. Singh (2018)**, "Deep learning methods for plant disease detection and diagnosis: A comprehensive survey," Computers and Electronics in Agriculture, vol. 151, pp. 38-49.
16. **Dyduch-Siemińska, M., Wawerska, K., & Gawroński, J**. **(2024)**. The Potential of Plant Tissue Cultures to Improve the Steviol Glycoside Profile of Stevia (Stevia rebaudiana Bertoni) Regenerants. International Journal of Molecular Sciences, 25(24), 13584. https://doi.org/10.3390/ijms252413584
17. **Luwańska, A.; Pérez, A.; Mańkowska, G.; Wielgus, K. (2025)**, Aplicación de cultivos in vitro de Stevia (Stevia rebaudiana Bertoni) en la obtención de material rico en glucósidos de esteviol. Herba Pol. 2015 , 61 , 50–63.
18. **Cámara de Diputados, "Stevia: Proceso de extracción y consumo**," [En línea]. Disponible: https://www.diputados.gob.mx/documentos/stevia. [Consultado: 27-sept.-2024].
19. **Jaramillo et al., (2017).** "Efecto de la producción de Stevia en México," Rev. Agroproductividad, vol. 10, no. 8, pp. 84-95.
20. **Barrow, N.J., Hartemink (2023)**, A.E. The effects of pH on nutrient availability depend on both soils and plants. Plant Soil 487, 21–37 https://doi.org/10.1007/s11104-023-05960-5.
21. **Garcia-Junior, M. A., Andrade, B. S., Lima, A. P., Soares, I. P., Notário, A. F. O., Bernardino, S. S., Guevara-Vega, M. F., Honório-Silva, G., Munoz, R. A. A., Jardim, A. C. G., Martins, M. M., Goulart, L. R., Cunha, T. M., Carneiro, M. G., & Sabino-Silva, R. (2025).** Artificial-Intelligence Bio-Inspired Peptide for Salivary Detection of SARS-CoV-2 in Electrochemical Biosensor Integrated with Machine Learning Algorithms. Biosensors, 15(2), 75. https://doi.org/10.3390/bios15020075
22. **Toor, M. S., Shahbaz, H., Yasin, M., Ali, A., Fitriyani, N. L., Kim, C., & Syafrudin, M. (2025).** An Optimized Weighted-Voting-Based Ensemble Learning Approach for Fake News Classification. Mathematics, 13(3), 449. https://doi.org/10.3390/math13030449
23. **Cepeda, S., Esteban-Sinovas, O., Singh, V., Shetty, P., Moiyadi, A., Dixon, L., Weld, A., Anichini, G., Giannarou, S., Camp, S., Zemmoura, I., Giammalva, G. R., Del Bene, M., Barbotti, A., DiMeco, F., West, T. R., Nahed, B. V., Romero, R., Arrese, I., ... Sarabia, R. (2025).** Deep Learning-Based Glioma Segmentation of 2D Intraoperative Ultrasound Images: A Multicenter Study Using the Brain Tumor Intraoperative Ultrasound Database (BraTioUS). Cancers, 17(2), 315. https://doi.org/10.3390/cancers17020315
24. **Liu, T. Y. A., Chen, H., Koseoglu, N. D., Kolchinski, A., Unberath, M., & Correa, Z. M. (2025).** Direct Prediction of 48 Month Survival Status in Patients with Uveal Melanoma Using Deep Learning and Digital Cytopathology Images. Cancers, 17(2), 230. https://doi.org/10.3390/cancers17020230
25. **N. A. Hussein, M. K. Ebrahim, and I. M. Khedr (2020)**, "Automatic plant disease detection using machine learning and image processing techniques," IEEE Access, vol. 8, pp. 195-202.
26. **R. Singh, T. Gupta, and M. P. Sharma (2019)**, "Neural network-based prediction of wheat yield under precision irrigation system," Journal of Precision Agriculture, vol. 10, no. 4, pp. 321-329, 2021. doi: 10.1007/s11119-021-09789-7.
27. **A. R. Khan, Z. Li, and P. Wang (2019)**, "Disease detection in potato crops using convolutional neural networks with multispectral images," Computers and Electronics in Agriculture, vol. 162, pp. 531-539,. doi: 10.1016/j.compag.2019.05.022.
28. **L. F. Rodríguez, M. O. Garcia, and J. S. Prieto (2020)**, "Nutrient deficiency detection in tomato plants using computer vision," Agricultural Systems, vol. 187, pp. 103-113. doi: 10.1016/j.agsy.2020.103022.
29. **H. Zhou, Q. Zhang, and J. Liao (2020)**, "Monitoring soybean growth using high-resolution imagery and neural networks," Remote Sensing, vol. 12, no. 8, pp. 1201-1210. doi: 10.3390/rs12081201.

30. **Atlas Scientific**. (n.d.). Wi-Fi Hydroponics Kit. Retrieved February 4, 2025, from https://atlas-scientific.com/kits/wi-fi-hydroponics-kit/
31. **P. Domingos (2012)**, "A Few Useful Things to Know About Machine Learning," Communications of the ACM, vol. 55, no. 10, pp. 78-87. doi: 10.1145/2347736.2347755.
32. **X. Liu, Y. Wang, and Q. Zhou (2021)**, "Image scaling and normalization techniques for precision agriculture," IEEE Access, vol. 9, pp. 14321-14332. doi: 10.1109/ACCESS.2021.3056789.
33. **Kim, Y., & Kim, S. (2024).** Automation and Optimization of Food Process Using CNN and Six-Axis Robotic Arm. Foods, 13(23), 3826. https://doi.org/10.3390/foods13233826
34. **M. Wahabzada, C. Mahlein, and U. Steiner (2015)**, "Plant phenotyping using segmentation and background elimination methods," Plant Methods, vol. 11, no. 1, p. 22. doi: 10.1186/s13007-015-0068-8.
35. **R. Lu (2022)**, "Data cleaning and preprocessing for agricultural AI systems," Journal of Agricultural Informatics, vol. 13, no. 3, pp. 112-123. doi: 10.17700/jai.2022.13.3.112.
36. **Mir, MA; Qazi, F.; Naseem, M.; Zia, SS; Agha, D.-S.; Mubeen, T. ,(2022).** Capa de invisibilidad mediante extracción de color y segmentación de imágenes con OpenCV. En Actas de la Conferencia mundial de 2022 sobre tecnologías inalámbricas y ópticas (GCWOT), Málaga, España, 14-17 de febrero de 2022; págs. 1-6.
37. J**eon, Y.-J., Park, S. J., Lee, H., Kim, H.-Y., & Jung, D.-H. (2024)**. Deep Learning-Based Model for Effective Classification of Ziziphus jujuba Using RGB Images. AgriEngineering, 6(4), 4604-4619. https://doi.org/10.3390/agriengineering6040263
38. **Boncelet, (2009).** C. Chapter 7—Image Noise Models. In The Essential Guide to Image Processing; Bovik, A., Ed.; Academic Press: Boston, MA, USA, 2009; pp. 143–167. ISBN 978-0-12-374457-9.
39. **Bi, C.; Zhang, S.; Chen, H.; Bi, X.; Liu, J.; Xie, H.; Yu, H.; Song, S.; Shi, L., (2024)** Non-Destructive Classification of Maize Seeds Based on RGB and Hyperspectral Data with Improved Grey Wolf Optimization Algorithms. Agronomy 2024, 14, 645.
40. **J. Brownlee, (2016)** Machine Learning Mastery with Python: Understand Your Data, Create Accurate Models, and Work Projects End-to-End, 2016.
41. **Yang, X., Zhang, J., Paneru, B., Lin, J., Bist, R. B., Lu, G., & Chai, L. (2025).** Precision Monitoring of Dead Chickens and Floor Eggs with a Robotic Machine Vision Method. AgriEngineering, 7(2), 35.https://doi.org/10.3390/agriengineering7020035
42. **Radočaj, P., Radočaj, D., & Martinović, G. (2025).** Optimizing Convolutional Neural Network Architectures with Optimal Activation Functions for Pediatric Pneumonia Diagnosis Using Chest X-rays. Big Data and Cognitive Computing, 9(2), 25. https://doi.org/10.3390/bdcc9020025
43. **Tammisetti, V., Stettinger, G., Cuellar, M. P., & Molina-Solana, M. (2025).** Meta-YOLOv8: Meta-Learning-Enhanced YOLOv8 for Precise Traffic Light Color Detection in ADAS. Electronics, 14(3), 468. https://doi.org/10.3390/electronics14030468
44. **Rey-Barroso, L., Vilaseca, M., Royo, S., Díaz-Doutón, F., Lihacova, I., Bondarenko, A., & Burgos-Fernández, F. J. (2025).** Training State-of-the-Art Deep Learning Algorithms with Visible and Extended Near-Infrared Multispectral Images of Skin Lesions for the Improvement of Skin Cancer Diagnosis. Diagnostics, 15(3), 355. https://doi.org/10.3390/diagnostics15030355
45. **Luque, A.; Carrasco, A.; Martín, A.; de las Heras, A., (2019)** The Impact of Class Imbalance in Classification Performance Metrics Based on the Binary Confusion Matrix. Pattern Recognit.91, 216–231.
46. **Chimate Y, Patil S, Prathapan K, Patil J, Khot J., (2025)** Optimized sequential model for superior classification of plant disease. Sci Rep.;15(1):3700. doi: 10.1038/s41598-025-86427-8. PMID: 39880879; PMCID: PMC11779840.

47. **Mohammed, F. A., Tune, K. K., Assefa, B. G., Jett, M., & Muhie, S. (2024).** Medical Image Classifications Using Convolutional Neural Networks: A Survey of Current Methods and Statistical Modeling of the Literature. Machine Learning and Knowledge Extraction, 6(1), 699-735. https://doi.org/10.3390/make6010033
48. **Sharshar, A., & Matsun, A. (2023).** Innovative horizons in aerial imagery: LSKNet meets DiffusionDet for advanced object detection. https://doi.org/10.48550/arXiv.2311.12956
49. **Mutawa, AM (2025).** Modelos híbridos de aprendizaje profundo basados en la atención para clasificar secuencias genómicas de COVID-19. AI, 6 (1), 4. https://doi.org/10.3390/ai6010004
50. **Primitivo, Díaz, Marco Pérez-Cisneros, Erik Cuevas, Octavio Camarena, Fernando Abraham Fausto Martínez, y Adrián González. (2018).** A Swarm Approach for Improving Voltage Profiles and Reduce Power Loss on Electrical Distribution Networks. IEEE Access 6: 49498-49512. https://doi.org/10.1109/ACCESS.2018.2868814.
51. **Moustafa, Maaskri, Mohamed Hamou Reda, y Adil Tomouh. (2022).** Ride Sharing Using Dynamic Rebalancing with PSO Clustering: A Case Study of NYC. Computación y Sistemas 26 (2): 963–975. https://doi.org/10.13053/CyS-26-2-3942.
52. **Benaissa, Safa, Reda Mohamed-Hamou, y Adil Toumouh. (2024)**. "Optimizing the Performance of the IDS through Feature-Relevant Selection Using PSO and Random Forest Techniques." Computación y Sistemas 28 (2): 473–488. https://doi.org/10.13053/CyS-28-2-4579.
53. **Liu, L., Yang, J., Yin, F., & He, L. (2025).** High-Resolution Mapping of Maize in Mountainous Terrain Using Machine Learning and Multi-Source Remote Sensing Data. Land, 14(2), 299. https://doi.org/10.3390/land14020299
54. **Abbasi, M., Váz, P., Silva, J. y Martins, P. (2025).** Enfoques de aprendizaje automático para predecir el rendimiento de la biomasa del maíz: aprovechamiento de la ingeniería de características y la integración integral de datos. Sustainability, 17 (1), 256. https://doi.org/10.3390/su17010256
55. **Mai, J., Lin, H., Hong, X., & Wei, Z. (2024).** Prediction of Potato Rot Level by Using Electronic Nose Based on Data Augmentation and Channel Attention Conditional Convolutional Neural Networks. Chemosensors, 12(12), 275. https://doi.org/10.3390/chemosensors12120275
56. **Ochoa, EJ, y Revilla, LC (2025).** Una red neuronal convolucional para la identificación temprana de arritmias supraventriculares. Actas de ingeniería , 83 (1), 8. https://doi.org/10.3390/ engproc2025083008
57. **Wang, H., Li, D., Li, Y., Zhu, G., & Lin, R. (2024).** Method for Remaining Useful Life Prediction of Turbofan Engines Combining Adam Optimization-Based Self-Attention Mechanism with Temporal Convolutional Networks. Applied Sciences, 14(17), 7723. https://doi.org/10.3390/app14177723
58. **Hwang, W. K., Jo, S. B., Han, D. E., Ahn, S. T., Oh, M. M., Park, H. S., Moon, D. G., Choi, I., Yang, Z., & Kim, J. W. (2025).** Artificial Intelligence-Based Classification and Segmentation of Bladder Cancer in Cystoscope Images. Cancers, 17(1), 57. https://doi.org/10.3390/cancers17010057
59. **Vrouva, S., Koumantakis, G. A., Sopidou, V., Tatsios, P. I., Raptis, C., & Adamopoulos, A. (2025).** Comparison of Machine Learning Algorithms and Hybrid Computational Intelligence Algorithms for Rehabilitation Classification and Prognosis in Reverse Total Shoulder Arthroplasty. Bioengineering, 12(2), 150. https://doi.org/10.3390/bioengineering12020150
60. **Keras. (s.f.).** MobileNet [Documentación]. Recuperado el 7 de enero de 2025, de https://keras.io/api/applications/mobilenet/
61. **Keras. (s.f.).** ResNet [Documentación]. Recuperado el 7 de enero de 2025, de https://keras.io/api/applications/resnet/

Article received on 01/02/2025; accepted on 16/06/2025.
**Corresponding author is Noel García-Díaz.*